Structural Phase Transitions and Cationic Motions in Pyridinium Dichloroiodate(I) as Studied by ^{1}H NMR, Differential Thermal Analysis, and Powder X-Ray Diffraction

Reiko Watanabe, Tetsuo Asaji, Yoshihiro Furukawa, and Daiyu Nakamura
Department of Chemistry, Faculty of Science, Nagoya University, Nagoya, Japan

Ryuichi Ikeda
Institute for Molecular Science, Myodaiji, Okazaki, Japan

Z. Naturforsch. **44a**, 1111–1115 (1989); received July 24, 1989

For crystals of pyridinium dichloroiodate(I), (pyH)ICl_2, the temperature dependences of the ^{1}H NMR spin-lattice relaxation time T_1 and the ^{1}H second moment M_2 were determined. M_2 was found to be small (~ 1 G^2) above room temperature, indicating that the cations perform rapid reorientational motion about their pseudohexad axis perpendicular to the cationic plane. ^{1}H T_1 at its minimum was unusually long, indicating this motion occurring in the low symmetry local environments. Phase transitions between stable solid phases were revealed at 282 and 373 K by the ^{1}H NMR measurements and differential thermal analysis. The highest-temperature phase was easily supercooled and transformed reversibly into another metastable phase and back on cooling and warming at almost the same temperature of 138 K. The kinetics of the phase transition from the supercooled to the stable phase at room temperature was analyzed using an Avrami type relation. The growth time of the stable phase was estimated to be about 14 h at room temperature.

1. Introduction

Reorientation of ions in crystals has extensively been studied by ^{1}H NMR and NQR experiments for the pyridinium cation (pyH^+) in (pyH)X (X = Cl, Br, I) [1–3], (pyH)AuX_4 (X = Cl, Br) [4, 5], and (pyH)$_2MX_6$ (M = Te, Sn; X = Cl, Br) [6–8]. In these crystals, except for (pyH)AuX_4, structural phase transitions have been detected and discussed [1–3, 6–8].

Recently [4] it was suggested that (pyH)AuX_4 (X = Cl, Br) has a glass-like state as to the orientation of the cations at lower temperatures, whereas at higher temperatures the cation behaves, because of its rapid reorientation, as if it had the C_6 symmetry. In the present investigation the motion of pyridinium cations in (pyH)ICl_2 crystals has been studied by means of ^{1}H NMR. To obtain information about the mechanism of the interesting phase transitions revealed and the unusual phases appearing, differential thermal analysis (DTA) and X-ray powder diffraction experiments have also been carried out.

Reprint requests to Prof. D. Nakamura, Dept. of Chemistry, Faculty of Science, Nagoya University, Nagoya 464-01, Japan.

2. Experimental

For the T_1 measurements, homemade pulsed NMR spectrometers already reported [9, 10] were employed at Larmor frequencies of 10.5, 20.0, and 36.5 MHz. A conventional 180°–τ–90° pulse sequence was used. To determine the ^{1}H NMR second moment M_2, resonance absorptions were recorded at 40 MHz by means of a JEOL JNM-MW-40 S broadline spectrometer equipped with a temperature controller. DTA was carried out with an apparatus already described [11]. X-ray powder patterns were recorded with a model VD-1A diffractometer from Shimadzu Co., equipped with a copper anticathode. X-ray photographs were taken at low temperatures by means of a Weissenberg camera. The powdered sample was sealed in a glass capillary with 0.5 mm diameter and placed in the flow of cold nitrogen gas of controlled temperature [12].

Copper vs. constantan thermocouples were used except for the low-temperature X-ray experiments, where a chromel vs. constantan thermocouple was employed. The observed temperatures were estimated to be accurate within ± 1 K for the pulsed NMR and DTA, ± 3 K for the broadline NMR, and ± 5 K for the high-temperature X-ray experiments. For the low-

0932-0784 / 89 / 1100-1111 $ 01.30/0. –

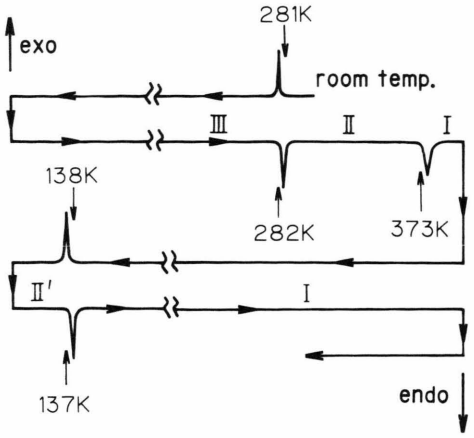

Fig. 1. DTA curves recorded for $(pyH)ICl_2$ crystals. Repeated cooling and heating runs were performed successively. The high-, room-, and low-temperature stable phases are denoted by I, II, and III, respectively. II′ indicates the low-temperature metastable phase.

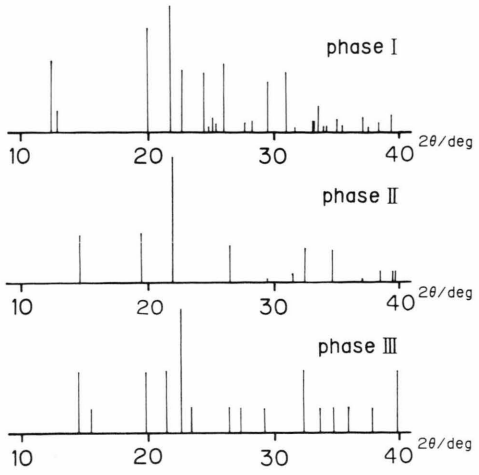

Fig. 2. X-ray powder patterns taken for the phases I, II, and III at ca. 375 K, room temperature, and ca. 243 K, respectively.

temperature X-ray experiments, the accuracy of the temperature determination was rather poor and estimated to be within ± 10 K.

$(pyH)ICl_2$ was prepared according to the method described in [13, 14] and purified by recrystallization from acetic acid. Anal. calc. for $(C_5H_6N)ICl_2$: C, 21.6%; H, 2.2%; N, 5.0%; Cl, 25.5%. Found: C, 21.6%; H, 2.0%; N, 5.0%; Cl, 25.3%.

3. Results and Discussion

a) DTA and X-Ray Powder Patterns

DTA curves repeatedly recorded while the sample temperature was increased and decreased are shown in Figure 1.When the temperature was lowered from room temperature, an exothermic anomaly appeared at 281 K. With increasing the temperature from ca. 100 K up to 410 K, endothermic anomalies appeared at 282 and 373 K. On the cooling run successively performed from 410 K, however, no heat anomaly was observed around 370 and 280 K but an exothermic anomaly could be observed at 138 K. With increasing the temperature again from ca. 100 K, an endothermic anomaly appeared at 137 K. However, the heat anomalies observed around 280 and 370 K in the second run (heating) could not be observed. These heat anomalies could not be recorded for a couple of hours on both heating and cooling runs once the sample was heated beyond ca. 370 K.

It becomes clear from the foregoing DTA experiments that there exist at least four solid phases below 410 K. The low-temperature stable phase III is transformed to the room-temperature phase II at 282 K, and the phase II to the high-temperature phase I at 373 K. Phase I is easily supercooled and transformed to the metastable low-temperature phase II′ at 138 K. Transformation between the supercooled phase I and phase II′ takes place reversibly. At room temperature, the supercooled phase I is transformed into the stable phase II with an extremely slow rate.

X-ray powder patterns observed for the stable phases I, II, and III are shown in Figure 2. Phase II, stable at room temperature, forms rhombohedral crystals belonging to the space group $R\bar{3}m$ with $a = 6.165$ Å, $\alpha = 82.45°$, and $Z = 1$ [15]. The present patterns for phase II correspond to these structural parameters.

b) ^1H NMR Spin-Lattice Relaxation Time and Second Moment

The temperature dependences of ^1H T_1 observed for the stable and metastable phases at the Larmor frequencies 10.5 and 36.5 MHz are shown in Figure 3. The dependency of T_1 on the Larmor frequency at lower temperatures suggests that the relaxation mechanism is dominantly governed by magnetic dipolar relaxation.

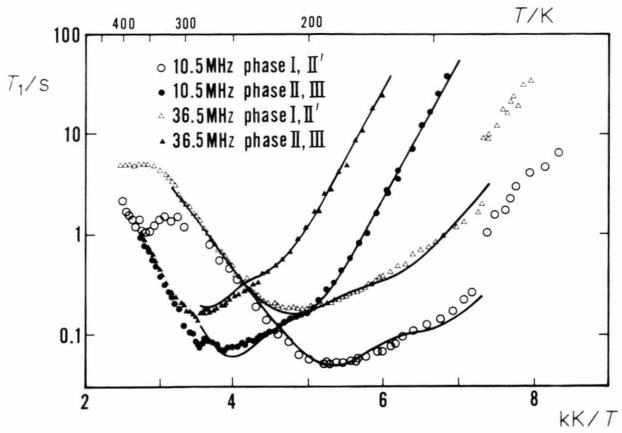

Fig. 3. Temperature dependences of ^{1}H T_1 observed at 10.5 and 36.5 MHz for several phases of $(pyH)ICl_2$. The Roman numerals indicate the same phases as defined in Figure 1. The best-fitted curves (see text) are shown by solid lines.

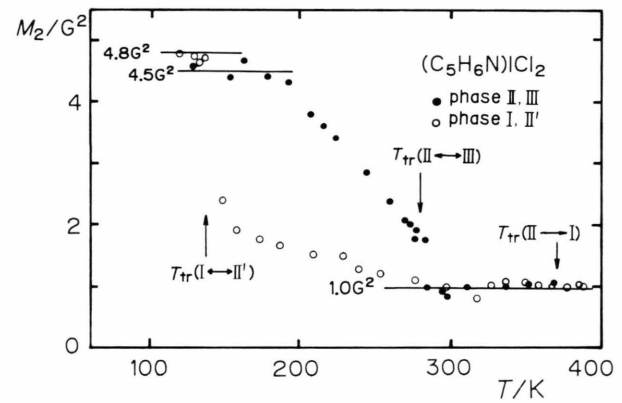

Fig. 4. Temperature dependence of ^{1}H NMR second moment M_2 observed for $(pyH)ICl_2$. Phase transition temperatures are indicated by arrows.

For phase III, an ^{1}H T_1 minimum of 68 ms was observed at 254 K at the Larmor frequency 10.5 MHz, whereas no T_1 minimum could be detected at 36.5 MHz. At the phase transition temperature between the phases II and III, a slight discontinuity in T_1 at both frequencies was observed. The T_1 minimum of 68 ms can be assigned to the reorientation of the cation around its pseudohexad axis C_6'. This assignment is supported by a large decrease (ca. 3.5 G^2) of M_2 with increasing temperature for the phases III and II as shown in Figure 4. Theoretically, a decrease of ca. 4.0 G^2 has been calculated for the onset of the C_6' reorientation of the cation [4, 12].

It should be noticed, however, that a much smaller T_1 minimum of ca. 25 ms than the 68 ms observed at the Larmor frequency of 10.5 MHz is expected from the observed decrease of M_2 by use of the simple BPP theory [16, 17]. Furthermore, it is unusual that the motional narrowing of the NMR absorption line was not completed at the temperature where the T_1 minimum was observed. Analogous features have been observed for various salts involving pyridinium cations [4, 12]. This has been explained by the in-plane orientations of the pyridinium cation being no longer equivalent energetically because of the differing electrostatic interactions between the electric dipole moment of the cation and the surrounding ions.

The hindering potential for the in-plane reorientation of the pyridinium cations in phase II should have the C_6 symmetry. This is because the cations in phase II are known to be located at positions having the site symmetry $\bar{3}$m [15]. The activation energy of 27 kJ mol^{-1} for the C_6' reorientation of the cations in this phase could be estimated from the gradient of the log T_1 vs. T^{-1} plot on the high-temperature side of the T_1 minimum by use of the BPP theory [16, 17].

From the X-ray powder photograph taken at ca. 240 K shown in Fig. 2, phase III was found to belong to monoclinic symmetry. The powder patterns could be interpreted by assuming a side-centered monoclinic lattice C with $a=8.96$, $b=8.37$, $c=5.77$ Å, and $\beta=98.8°$.

A comparison between the observed and calculated 2θ values given in Table 1 shows the adequacy of the above structure. The cell volume (214 Å^3) of the primitive lattice of phase III is slightly smaller than that (229 Å^3) of the room-temperature rhombohedral cell. Therefore, it is expected that the barrier to reorientation of the cation is higher in phase III than in phase II.

For the supercooled phase I, an ^{1}H T_1 minimum of 53 ms was observed at ca. 185 K at the Larmor frequency 10.5 MHz. The T_1 minimum observed is considerably longer than the estimated one (25 ms) for the C_6' reorientation of the cation from the BPP theory [16, 17] based on the observed M_2 decrease. This suggests that the correlation times for the reorientational motion are distributed over a fairly wide range, or that hindering barriers to the reorientation of the cation differ, as already revealed for the pyridinium cation in some complex crystals [4]. In fact, the X-ray powder patterns of the supercooled phase I were more complex than those of phase II (cf. Fig. 2), suggesting that the crystal symmetry is lower in phase I than in

Table 1. Comparison between observed and calculated 2θ values for phase III of $(pyH)ICl_2$ (see text).

$h\ k\ l$	$2\theta_{calc}$	$2\theta_{obs}$	$h\ k\ l$	$2\theta_{calc}$	$2\theta_{obs}$
1 1 0	14.56	14.55	3 1 0	32.16	32.32
0 0 1	15.54	15.52	1 1 $\bar{2}$	33.27	–
2 0 0	20.06	19.82	1 3 0	33.68	33.59
$\bar{1}$ 1 1	20.20	–	3 1 $\bar{1}$	33.73	–
0 2 0	21.23	21.44	2 0 $\bar{2}$	34.72	34.67
1 1 1	22.46	22.60	2 2 1	34.86	–
2 0 $\bar{1}$	23.48	23.43	1 1 2	36.17	35.94
0 2 1	26.42	26.38	$\bar{1}$ 3 1	36.60	–
2 0 1	27.33	27.25	3 1 1	37.96	37.83
2 2 0	29.37	29.21	1 3 1	37.96	
0 0 2	31.37	–	0 2 2	38.19	–
$\bar{2}$ 2 1	31.86	–	2 0 2	40.15	39.87

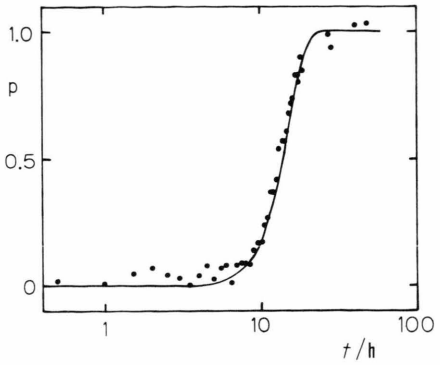

Fig. 5. Time dependence of the fraction p of the stable room-temperature phase observed for $(pyH)ICl_2$ at room temperature. Solid line indicates the best-fitted curve (see text).

phase II. This means that the cation in the supercooled phase I reorients between potential wells having different depths corresponding to a lower crystal symmetry, whereas the cation in phase II performs C_6' reorientation between potential wells of equal depth consistent with the site symmetry of the cation. The fact that the V-shaped $\log T_1$ vs. T^{-1} curve observed for the supercooled phase I is asymmetric and has a milder gradient on the low-temperature side of the minimum supports this picture.

The shallow minima of the ^1H T_1 curves of phase III and the supercooled phase I were interpreted [12] by assuming an asymmetric potential function as successfully employed for the fitting of the ^1H T_1 data of $(pyH)AuCl_4$ [4]. We employed here the same treatment. In the present calculation, three activation energies E_A, E_B, and E_C were introduced for the reorientation of the cations correspoding to three nonequivalent hindering barriers. The fitting was carried out using a program SALS [18]. The obtained theoretical curves are shown in Figure 3.

The best-fitted parameters for phase III became $E_A = 30.3$, $E_B = 26.6$, $E_C = 22.4$ kJ mol^{-1}, $K^{-1} = 3.4 \times 10^{-14}$ s (K denotes the transition probability rate at infinite temperature [4]); for the supercooled phase I they were $E_A = 20.6$, $E_B = 18.3$, $E_C = 15.0$ kJ mol^{-1}, $K^{-1} = 1.1 \times 10^{-13}$ s, and $\Delta M_2 = 3.6$ G^2. Here, ΔM_2 of phase III was fixed to the observed value of 3.5 G^2. The activation energies obtained are larger for phase III than for the supercooled phase I, indicating that the cations are more tightly bound in the former phase than in the latter.

c) Kinetics of the Phase Transition from the Supercooled Phase I to Phase II at Room Temperature

The kinetics of the phase transformation from the supercooled phase I to phase II was studied at ca. 300 K by use of ^1H T_1 measurements at 20 MHz. A similar application of pulsed NMR for the study of the kinetics of phase transitions has been reported by Miyajima et al. [19].

The ^1H spin-lattice relaxation times and the equilibrium values of the nuclear magnetization M_z are denoted as T_{1s} and M_0^s for the stable phase II and as T_{1m} and M_0^m for the metastable (supercooled) phase I. The mole fraction of the grown phase II domains or the extent of the progress of the phase transition is denoted by p. When the $180° - \tau - 90°$ pulse sequence was employed, the recovery of $M_z(\tau)$ as a function of the spacing time τ can be written as [19]

$$\frac{M_0 - M_z(\tau)}{2M_0} = \frac{p\alpha \exp(-\tau/T_{1s}) + (1-p)\exp(-\tau/T_{1m})}{p\alpha + (1-p)}, \quad (1)$$

where

$$\alpha = M_0^s/M_0^m, \quad (2)$$

$$M_0 = pM_0^s + (1-p)M_0^m. \quad (3)$$

Here we assume that p is constant while a T_1 measurement is performed (ca. 5 min).

T_{1s} and T_{1m} could be determined to be 0.14 and 1.45 s, respectively, from the ^1H T_1 experiments carried out at ca. 300 K and 20.0 MHz. Since the two spin-lattice relaxation times are sufficiently separated, p is easily estimated by assuming $\alpha = 1$. The sample

heated up to ca. 400 K was quenched down to ca. 300 K and, then the observation of the change of the magnetization recovery curves was followed as a function of the time. The experimental values of p thus obtained are plotted in Figure 5.

The evolution of the stable phase fraction p can be well explained by the Avrami type relation [20–22]

$$p = 1 - \exp\{-(t/\tau_g)^n\} . \quad (4)$$

This equation, based on a homogeneous nucleation-and-growth mechanism, was developed by Johnson and Mehl [19, 23]. Here, τ_g can be defined as the growing time of the stable phase. By fitting (4) to the observed values as indicated in Fig. 5, $n = 3.9$ and $\tau_g = 5 \times 10^4$ s were obtained. The observed values agree very well with the calculated curve. The growing time τ_g is extremely long and approximately equal to 14 h at room temperature.

Acknowledgement

This work was partly supported by a research grant from Nippon Sheet Glass Foundation for Materials Science.

[1] C. H. Matthews and D. F. R. Gilson, Can. J. Chem. **48,** 2625 (1970).
[2] J. A. Ripmeester, Can. J. Chem. **54,** 3453 (1976).
[3] J. A. Ripmeester, J. Chem. Phys. **85,** 747 (1986).
[4] Y. Ito, T. Asaji, R. Ikeda, and D. Nakamura, Ber. Bunsenges. Phys. Chem. **92,** 885 (1988).
[5] A. Ishikawa, Y. Ito, K. Horiuchi, T. Asaji, and D. Nakamura, J. Mol. Struct. **192,** 221 (1989).
[6] Y. Ito, T. Asaji, and D. Nakamura, phys. stat. sol. (a) **104,** K 97 (1987).
[7] Y. Tai, A. Ishikawa, K. Horiuchi, T. Asaji, D. Nakamura, and R. Ikeda, Z. Naturforsch. **43a,** 1002 (1988).
[8] Y. Tai, T. Asaji, R. Ikeda, and D. Nakamura, Z. Naturforsch. **44a,** 300 (1989).
[9] L. S. Prabhumirashi, R. Ikeda, and D. Nakamura, Ber. Bunsenges. Phys. Chem. **85,** 1142 (1981).
[10] S. Gima, Y. Furukawa, R. Ikeda, and D. Nakamura, J. Mol. Struct. **111,** 189 (1983).
[11] Y. Kume, R. Ikeda, and D. Nakamura, J. Magn. Reson **33,** 331 (1979).
[12] R. Watanabe, M. Sc. Thesis, Nagoya University 1988.
[13] F. D. Chattaway and F. L. Garton, J. Chem. Soc. **1924,** 183.
[14] Y. Kurita, D. Nakamura, and N. Hayakawa, J. Chem. Soc. Japan **79,** 1093 (1958).
[15] P. A. Tucker and P. A. Kroon, Acta Crystallogr. **B 29,** 2967 (1973).
[16] N. Bloembergen, E. M. Purcell, and R. V. Pound, Phys. Rev. **73,** 679 (1948).
[17] G. Soda and H. Chihara, J. Phys. Soc. Japan **36,** 954 (1974).
[18] Y. Oyanagi and T. Nakagawa, Program Library in Nagoya University Computation Center, code number 466.
[19] S. Miyajima, N. Nakamura, and H. Chihara, J. Chem. Soc., Faraday Trans. **78,** 577 (1982).
[20] M. Avrami, J. Chem. Phys. **7,** 1103 (1939); **8,** 212 (1940); **9,** 177 (1941).
[21] M. Hashimoto and Al. Weiss, J. Mol. Struct. **58,** 243 (1980).
[22] C. N. R. Rao and J. Gopalakrishnan, New Directions in Solid State Chemistry, p. 162, Cambridge University Press 1986.
[23] W. A. Johnson and R. F. Mehl, Trans. Amer. Inst. Min. Metall. Pet. Eng. **135,** 416 (1939).